WFUMB Ultrasound Open 2 (2024) 100035

Contents lists available at ScienceDirect

WFUMB Ultrasound Open

journal homepage: www.journals.elsevier.com/wfumb-ultrasound-open

Original Contribution

Total signal intensity of ultrasound laboratory vertical artifacts: A semi-quantitative tool

Joao Leote [a,b,*], Ricardo Loução [c], Madalena Aguiar [b], Mariana Tavares [b], Paloma Ferreira [b], Tiago Muxagata [b], Diana Guerreiro [b], Hermínia Dias [b], Jacobo Bacariza [a], Filipe Gonzalez [a]

[a] Critical Care Department, Hospital Garcia de Orta EPE, Almada, Portugal
[b] Escola Superior de Tecnologia da Saúde de Lisboa, Instituto Politécnico de Lisboa, Lisboa, Portugal
[c] Centre for General Neurosurgery, University Hospital Cologne, Cologne, Germany

ARTICLE INFO

Handling Editor: Prof. MD Manjiri Dighe

Keywords:
Lung ultrasound
Vertical artifacts
Total intensity
Semi-quantitative

ABSTRACT

Quantitative approaches to improve lung ultrasound (LUS) vertical artifacts (VA) interpretation using total signal intensity (I_{TOT}) are not widely available for clinical practice. In this study, we aimed to i) develop a mathematical algorithm to extract I_{TOT} as a post-hoc LUS analysis and ii) confirm I_{TOT} utility by conducting laboratory VA research using an *in vitro* model with different acoustic channels.

The I_{TOT} was extracted from static and conventional LUS imaging recorded from *in vitro* models after varying the amount of water content or the pores size of the phantom, compared to a control condition.

The defined algorithm was able to calculate the I_{TOT} from all phantoms. Mean I_{TOT} showed statistically significantly different values across phantom categories.

We demonstrate that I_{TOT} may be able to differentiate the *in vitro* acoustic channels formed by increased water content from those with small size pores. However, the utility of this semi-quantitative tool in clinical practice or other LUS imaging data sets remains unclear.

1. Introduction

The usefulness of lung ultrasound (LUS) as a monitoring tool increased worldwide after the COVID-19 pandemic, mainly in intensive care and emergency settings [1]. LUS enables monitoring of the lung interstitium for changes in aeration loss patterns by identifying B-lines, white lung patterns, and consolidations [1,2]. These features compose the majority of LUS scores validated in pneumonia [2] and reflect the increasing inflammatory interstitial edema seen during the time course of severe acute distress respiratory syndrome (ARDS) [1,2]. In addition to pleural effusion in heart failure [2], diffuse B-lines were also recognized in acute coronary syndrome when associated with cardiogenic pulmonary edema [3].

In the last few years, several advances have been achieved regarding the biophysics of the B-lines. Despite their relevance as a marker of regional lung deaeration, vertical artifacts (VA) cannot be entirely explained by the lung interstitial edema [4,5]. Consequently, a recent consensus established technical ultrasound (US) settings that must be considered and reported for an adequate VA evaluation in clinical practice [6,7]. The present knowledge about VA modulates the clinical practice interpretation, whereas in the past, their presence almost every time meant increased lung interstitial fluid, reported as lung B-lines [1].

Recently, Mento et al. [8] reviewed the literature and suggested that quantitative approaches to LUS data, like spectroscopy [9], should improve VA clinical interpretation in the future. Previously, Mento and colleagues [10] described a multifrequency LUS approach to record VA with a linear probe after defining sequential probe pulses with different center frequencies (3, 4, 5 and 6 MHz) via a programmable platform [11]. They then, extracted the mean native frequency, mean bandwidth and mean total signal intensity (I_{TOT}) to differentiate pulmonary fibrosis VA from pulmonary edema VA. The authors [10] based their reasoning on the higher attenuation of LUS echoes in patients with increased fibrotic content (i.e. pulmonary fibrosis) rather than those with water or inflammatory fluids (i.e. pulmonary edema). In fact, using the metric of I_{TOT}, the researchers were able to detect the lower intensity VA from patients with pulmonary fibrosis with a sensitivity and specificity of 92%. Despite their significant findings, such methodology is not widely available.

* Corresponding author. Critical Care Department, Hospital Garcia de Orta EPE, Almada, Portugal.
E-mail address: jlleotte@gmail.com (J. Leote).

https://doi.org/10.1016/j.wfumbo.2024.100035
Received 13 October 2023; Received in revised form 7 February 2024; Accepted 8 February 2024
Available online 8 February 2024

For this reason, we defined a mathematical algorithm to further validate the I_{TOT} as a *post-hoc* LUS analysis. Secondly, we performed laboratory VA experiments with different acoustic traps to confirm the utility of I_{TOT}.

2. Material and methods

We created an *in vitro* model to generate VA [12,13] from structures with different porosities. The superficial layer consisted of a mixture of gelatin and sugar-free Metamucil with a ratio of 3:1 per liter of water to recreate the subcutaneous tissue with 2 cm of thickness. To simulate the well-defined and homogenous pleura, a translucent plastic was applied. For the air-lung interface, as reported by others [13,14], we used two damp sponges after evaluating their pores and septa size through electron microscopy (Fig. 1). The first sponge had 278 μm mean-diameter pores (±106 μm), intertwined by 10 μm septa. The second sponge had 190 μm mean-diameter pores (±70 μm), also spaced by 10 μm septa. The two different pore size sponges were selected to produce different intensity echo reflections as already reported in the *in vitro* experiments [8,10,11]. The mean pore and septa sizes were extracted from ten photographs of each sponge. Consequently, water was added to the sponges as follows: i) to the first sponge, 10 mL of water to obtain the control phantom (Fig. 1B) and 30 mL of water to obtain the flooded phantom (Fig. 1B); ii) to the smaller pore sponge phantom (Fig. 1C), 10 mL of water. We constructed ten phantoms of each phantom category. An iron structure 10 cm high and a metal base with a flexible aluminum arm at the top were used to fixate the probe over the phantoms without movement (Fig. 1) To warrant a motionless probe during recordings, a gyroscope was attached to the iron structure as reported previously [13].

For US image acquisition, the MicrUs EXT-1H beamformer (Telemed, Vilnius, Lithuania) was used to produce echo waves through a microcurvilinear probe with a 20-mm radius and 5 mm lateral dimension, system frequency of 4 MHz, field of view of 46[a] or 97 mm with a focal length of 20 mm, with 64 piezoelectric elements (code MC8-4R20S-3, Telemed). The US signal was recorded with a 40 MHz bandwidth sampling frequency, a frame rate up to 120 Hz and the signal was converted to digital using an 8-bit converter before being exported in DICOM format.

US images were recorded using the following settings: mechanical index of 0.5; depth of 70 mm; one focal depth (on the gelatin to sponge interface); the power of −10 dB; gain of 90%; equal level of time gain compensation across depth, standard line density, a dynamic range of 66 dB, without tissue equalization or optional post-processing tools. DICOM clips were recorded with 5 s duration and the first 30 frames of each clip were excluded to ensure the stable performance of the probe.

In the *in vitro* static models, VAs were defined as triangular shape with a vertex originating from the homogenous 'pleural line', extending to the triangle base on the bottom of the screen, blurring reverberation artifacts. For the small pore phantom and control phantom categories, US images were selected if they showed one or two VAs, and for the flooded phantom category, images with at least five VAs were selected.

The I_{TOT} (dB) was calculated as described in equation (1) [10]:

$$I_{TOT} = 20\ log_{10}\left(A_{pix}\sum_{i,j}10^{\frac{ROI_{B(i,j)}}{20}}\right) \quad \text{Eq. 1}$$

where A_{pix} is the area of a pixel (3.6×10^{-3} mm^2), i and j indexes refer to the pixel in ROI_B located at the i-th row and j-th column, and $ROI_B(i,j)$ is the intensity value (in dB) of the pixel located at the i-th row and j-th column. After computing the US intensity signal, an empirically determined threshold of −20dB was defined to reduce the influence of data noise.

This was computed in MATLAB (MathWorks, MA, USA) algorithm (available in supplementary material). The maximum signal amplitude from the region of interest (ROI) was used as the reference value. The ROIs were drawn three times around different VA within each phantom to ensure data reproducibility. Two authors (MT and JL), were instructed to manually draw the ROIs within the inner border of the VA (Fig. 2) from the upper part including the 'pleura' mimic line to the bottom part of the US image.

Mean I_{TOT} was calculated from 3 ROI measurements. The average I_{TOT} were compared using the One-Way ANOVA test after satisfying test assumptions. Statistical analyses were performed using SPSS Statistics, version 24 (IBM, Armonk, NY, USA). A p-value $<.05$ was considered to indicate statistical significance.

3. Results

Fig. 2 shows an example of each US imaging recorded for each phantom category. The defined algorithm was able to calculate the I_{TOT} of the selected ROIs from all phantoms. The algorithm was shown in supplementary material (algorithm files, 1 to 3). Fig. 2B shows a boxplot chart with the descriptive statistics of the mean I_{TOT} in each attempt grouped by phantom categories. In addition, Table 1 also shows the 95% confidence interval of mean I_{TOT}. On the first attempt (left boxplot on Fig. 2B), mean I_{TOT} showed statistically significantly different values across phantom categories (Welch's $F(2, 14.777) = 78{,}985$; $p < .0005$). In this attempt, there was an increase in mean I_{TOT} from $-14{,}9 \pm 2{,}6$ in the small pore phantom category to $-6{,}0 \pm 0.6$ in the flooded phantom category and to $-9{,}3 \pm 1{,}2$ in the control phantom category ($p < .0005$). The statistics of all attempts showed similar results and were described inTables 1 and 2 of the supplementary material (tables).

4. Discussion

Our main findings were the development of a semi-quantitative, *post-hoc* open tool able to extract the I_{TOT} from VA obtained with conventional US imaging instead of using a more complex US acquisition system. Secondly, we confirmed previous observations [10] that the I_{TOT} of

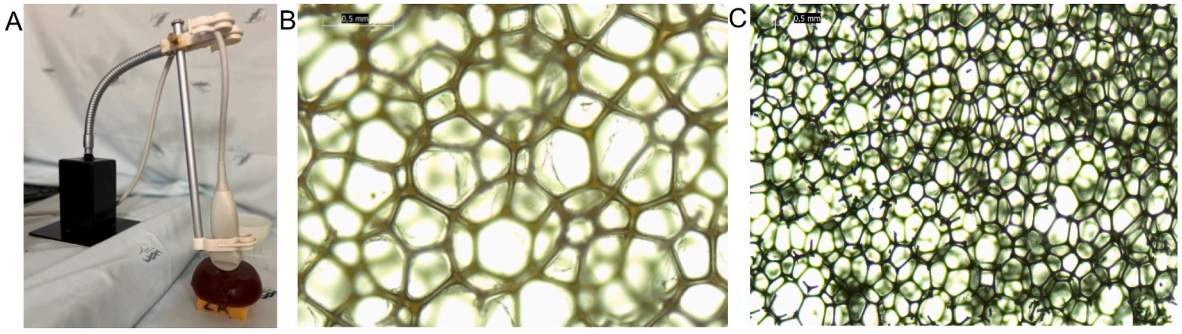

Fig. 1. Experimental setup with a custom probe holder above the phantom (A). The *in vitro* model was based on two sponges (B, C) placed below a gelatin/metamucil mixture.

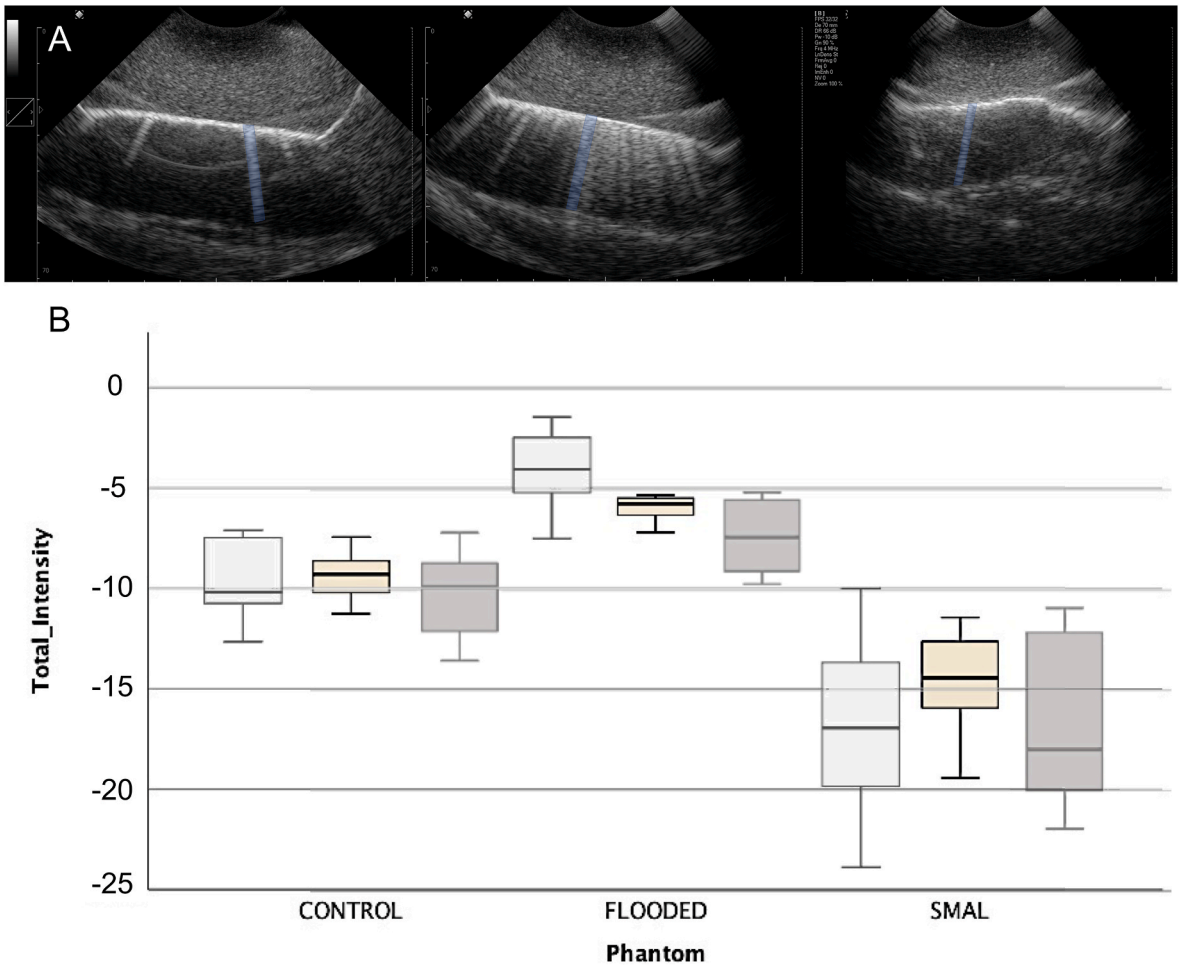

Fig. 2. An ultrasound frame example of each phantom variant. Note the vertical artifacts (VA) present in control phantom (left image), flooded phantom (middle image) and small pore phantom (right image). On each frame, was showed an example of the selected regions of interest (ROI) in blue. The lateral parts of the models with irregular "pleura" were ignored. Total signal intensity of the VA extracted from ten phantoms of each variant and ROIs were drawn three times for different VA. (For interpretation of the references to colour in this figure legend, the reader is referred to the Web version of this article.)

Table 1
Descriptive statistics from total signal intensity extracted from a category of phantom's (N = 10), named as a control phantom group (CP) flooded phantom group (FP) and small pore phantom group (SP). The total intensity was extracted after selecting a region of interest that included the vertical artifact. This procedure was done three times (attempts from #1 to #3) using different vertical artifacts.

Total Intensity/Attempt	Phantom			95% Confidence Interval			
		Mean (SD)	Std. Error	Lower bound	Upper bound	Min.	Max.
#1	CP	−9.33 (1.16)	0.36	−10.16	−8.50	−11.25	−7.43
	FP	−5.94 (0.59)	0.19	−6.36	−5.52	−7.19	−5.35
	SP	−14.88 (2.60)	0.82	−16.73	−13.02	−19.43	−11.43
#2	CP	−9.58 (1.98)	0.63	−11.00	−8.16	−12.69	−7.14
	FP	−4.24 (2.05)	0.65	−5.70	−2.77	−7.56	−1.50
	SP	−16.62 (4.35)	1.38	−19.73	−13.50	−23.91	−10.04
#3	CP	−10.23 (2.24)	0.70	−11.83	−8.62	−13.54	−7.14
	FP	−7.18 (1.75)	0.55	−8.43	−5.92	−9.70	−5.12
	SP	−16.92 (4.22)	1.33	−19.94	−13.90	−21.90	−10.89

CP – Control Phantom; FP – Flooded Phantom; SD – Standard deviation SP – Small pore Phantom; STD – Standard.

VA is dependent on the amount of water content and pore diameter.

LUS in clinical practice is based on a qualitative and subjective evaluation. Nonetheless, recent developments suggest using quantitative approaches to estimate the alveolar geometry and lung surface roughness after varying the probe's center frequency [8–10,15,16]. VA is generated by the reflection of the emitted echo waves, where they can penetrate (due to low tissue impedance), producing scatters that bounce backward towards the US probe [5,14]. The reflection intensity from the scattering is influenced by the three-dimensional volume and geometry of the object through which the echo waves have passed [15,16]. In our work, we used the water volume within two different spaces (dimension and geometry) allowing echo waves transmission by decreasing the amount of attenuated waves along the *in vitro* model depth (i.e. acoustic channel).

We were able evaluate the different scattering spaces content after recording US imaging with a curvilinear probe with a system frequency of 4 MHz from three groups of *in vitro* phantom categories. VA obtained from phantom categories were morphologically different (Fig. 1). In the control condition, the VA showed hyperechoic homogenous horizontal lines parallel to the 'pleura', whereas after increasing the water content, confluent VAs were shown to have lower echogenicity and broadening width with depth. On the other hand, after decreasing the pore's size diameter, VAs showed sparse and non-homogenous lines in the deeper part. Our findings are concordant with the numerous *in vitro*, *ex vivo*, and *in vivo* reports [9] that concluded that the VA morphology varies after altering the porosity (or density), alveolar geometry [15], and tissue roughness [16].

In our study, VA offline analysis was done to extract the I_{TOT} after delineating an ROI from the 'pleura' line (considered the $I_{TOT} = 0$ dB) until the end of the VA on depth. Due to the definition of I_{TOT}, different sizes of ROI might lead to different I_{TOT} values. A robust definition of the ROI is therefore crucial to ensure comparability of results. In this work, we extended the ROI to the end of the image, sometimes including pixels without any visually appreciable artifact towards the outer border of the image. To reduce the influence of such pixels, an empirically determined threshold of −20 dB was applied, removing pixels with intensity lower than −20 dB.

The mean values of I_{TOT} revealed a distinct pattern between the two tested phantom categories (large pores with high water content versus small pores with low water content). When increasing the water content, the confluent VA led to I_{TOT} more closely related to the 'pleura' line signal. Whereas the roughly and sparsely defined VA after decreasing the size of the pores led to a hypoechoic signal, with high mean I_{TOT} (more negative in relation to the 'pleura' line signal). Mento et al. [10], described the utility of this measure to provide an indirect estimation of the air spaces' dimensions either in fibrotic lungs [10] or experimental models with peripheral air-space dimensions above 340 μm [16], although VAs were recorded using a sequence of frequencies. In this study, we used a conventional system to record US images.

We chose to use I_{TOT} as the central parameter of this study due to its quantitative nature. In a clinical setting, using a quantitative measure can not only remove potential subjective biases but also allow inter-site comparability. In fact, implementing these 'online' measures could provide bedside insight into lung density. During I_{TOT} calculation, we applied a −20dB empirical threshold upon inspection of the recorded LUS images, where the background noise was determined to be around the −20dB level. Applying the threshold means that pixels below this value were not included in the I_{TOT} which falls in line with previous reports of I_{TOT} [9,10,16]. In further studies, the data noise removal should use standardized post-processing tools for systematical evaluation of the noise level.

LUS VA morphology may vary with pleural irregularities, probe center frequency, probe type, US settings, alveolar geometry and content [4,5,10]. Therefore, the utility of the described tool in either other US imaging data sets or clinical practice remains unproven.

In sum, we described the utility of the I_{TOT} to provide information about acoustic channels content that originate LUS VA after using a *post-hoc* and semi-quantitative tool.

Data availability

The authors partially provided data in the supplementary material. The rest of it, will be available on request.

Declaration of competing interest

The authors have nothing to declare.

Acknowledgments

The authors would like to express their gratitude to Mário Matos for the time dispended on sponge electronic microscopy.

Appendix A. Supplementary data

Supplementary data to this article can be found online at https://doi.org/10.1016/j.wfumbo.2024.100035.

References

[1] Pecho-Silva S, Navarro-Solsol AC, Taype-Rondan A, Torres-Valencia J, Arteaga-Livias K, Herriman DA, Acosta-Pinzas K, Valenzuela-Rodriguez G, Barboza JJ, Panduro-Correa V. Pulmonary ultrasound in the diagnosis and monitoring of coronavirus disease (COVID-19): a systematic review. Ultrasound Med Biol 2021; 47:1997–2005. https://doi.org/10.1016/j.ultrasmedbio.2021.04.011.

[2] Neuteboom OB, Heldeweg ML, Pisani L, Smit MR, Lagrand WK, Cherpanath TG, Dondorp AM, Schultz MJ, Tuinman PR. Assessing extravascular lung water in critically ill patients using lung ultrasound: a systematic review on methodological aspects in diagnostic accuracy studies. Ultrasound Med Biol 2020;46:1557–64. https://doi.org/10.1016/j.ultrasmedbio.2020.02.014.

[3] Lindner M, Lindsey A, Bain PA, Platz E. Prevalence and prognostic importance of lung ultrasound findings in acute coronary syndrome: a systematic review. Echocardiography 2021;38:2069–76. https://doi.org/10.1111/echo.15262.

[4] Soldati G, Smargiassi A, Demi L, Inchingolo R. Artifactual lung ultrasonography: it is a matter of traps, order, and disorder. Appl Sci 2020;10:1570. https://doi.org/10.3390/app10051570.

[5] Demi M. On the replica of US pulmonary artifacts by means of physical models. Diagnostics 2021;11:1666–78. https://doi.org/10.3390/diagnostics11091666.

[6] Demi L, Wolfram F, Klersy C, De Silvestri A, Ferretti VV, Muller M, Miller D, Feletti F, Wełnicki M, Buda N, Skoczylas A, Pomiecko A, Damjanovic D, Olszewski R, Kirkpatrick AW, Breitkreutz R, Mathis G, Soldati G, Smargiassi A, Inchingolo R, Perrone T. New international guidelines and consensus on the use of lung ultrasound. J Ultrasound Med 2023;42:309–44. https://doi.org/10.1002/jum.16088.

[7] Laursen CB, Clive A, Hallifax R, Pietersen PI, Asciak R, Davidsen JR, Bhatnagar R, Bedawi EO, Jacobsen N, Coleman C, Edey A, Via G, Volpicelli G, Massard G, Raimondi F, Evison M, Konge L, Annema J, Rahman NM, Maskell N. European Respiratory Society statement on thoracic ultrasound. Eur Respir J 2021;57: 2001519. https://doi.org/10.1183/13993003.01519-2020.

[8] Demi L, van Hoeve W, van Sloun RJG, Soldati G, Demi M. Determination of a potential quantitative measure of the state of the lung using lung ultrasound spectroscopy. Sci Rep 2017;7:12746. https://doi.org/10.1038/s41598-017-13078-9.

[9] Mento F, Khan U, Faita F, Smargiassi A, Inchingolo R, Perrone T, Demi L. State of the art in lung ultrasound, shifting from qualitative to quantitative analyses. Ultrasound Med Biol 2022;48:2398–416. https://doi.org/10.1016/j.ultrasmedbio.2022.07.007.

[10] Mento F, Soldati G, Prediletto R, Demi M, Demi L. Quantitative lung ultrasound spectroscopy applied to the diagnosis of pulmonary fibrosis: the first clinical study. IEEE Trans Ultrason Ferroelectrics Freq Control 2020;67:2265–73. https://doi.org/10.1109/TUFFC.2020.3012289.

[11] Tortoli P, Bassi L, Boni E, Dallai A, Guidi F, Ricci S. ULA- OP: an advanced open platform for ultrasound research. IEEE Trans Ultrason Ferroelectrics Freq Control 2009;56:2207–16.

[12] Blüthgen C, Sanabria S, Frauenfelder T, Klingmüller V, Rominger M. Economical sponge phantom for teaching, understanding, and researching A- and B-line reverberation artifacts in lung ultrasound. J Ultrasound Med 2017;36:2133–42. https://doi.org/10.1002/jum.14266.

[13] Leote J, Muxagata T, Guerreiro D, Francisco C, Dias H, Loução R, Bacariza J, Gonzalez F, EchoCrit Group. Influence of ultrasound settings on laboratory vertical artifacts. Ultrasound Med Biol 2023;49:1901–8. https://doi.org/10.1016/j.ultrasmedbio.2023.03.018.

[14] Soldati G, Giunta V, Sher S, Melosi F, Dini C. "Synthetic" comets: a new look at lung sonography. Ultrasound Med Biol 2011;37:1762–70. https://doi.org/10.1016/j.ultrasmedbio.2011.05.024.

[15] Peschiera E, Mento F, Demi L. Numerical study on lung ultrasound B- line formation as a function of imaging frequency and alveolar geometries. J Acoust Soc Am 2021;149:2304–11. https://doi.org/10.1121/10.0003930.

[16] Mento F, Perini M, Malacarne C, Demi L. Ultrasound multifrequency strategy to estimate the lung surface roughness, in silico and in vitro results. Ultrasonics 2023; 135:107143. https://doi.org/10.1016/j.ultras.2023.107143. 24.